Gold Bull (2014) 47:245–253
DOI 10.1007/s13404-014-0147-8

ORIGINAL PAPER

Gold nanoparticle synthesis using the thermophilic bacterium *Thermus scotoductus* SA-01 and the purification and characterization of its unusual gold reducing protein

Mariana Erasmus · Errol Duncan Cason · Jacqueline van Marwijk · Elsabé Botes · Mariekie Gericke · Esta van Heerden

Published online: 6 August 2014

Abstract Nanoparticles are very important materials for implementing nanotechnology in diverse areas and are abundant in nature as living organisms operate at a nanoscale. As nanoparticles exhibit interesting size- and shape-dependent physical and chemical properties, the synthesis of uniform nanoparticles with controlled sizes and shapes is of great importance. Nanoparticles are the end products of a wide variety of physical, chemical and biological processes, some of which are novel and radically different and others of which are quite commonplace. The ability to produce nanoparticles with specific shapes and controlled sizes could result in interesting new applications that can potentially be utilized in areas such as optics, electronics and the biomedical field. In the present study, we have demonstrated the ability of the thermophilic bacterium *Thermus scotoductus* SA-01 to synthesize gold nanoparticles and determined the effect of the physico-chemical parameters on particle synthesis. Furthermore, a protein purified from this bacterium is shown to be capable of reducing $HAuCl_4$ to form elemental nanoparticles in vitro. The protein was purified to homogeneity and identified through N-terminal sequencing as an ABC transporter, peptide-binding protein. It is speculated that this protein reduces Au(III) through an electron shuttle mechanism involving a cysteine disulphide bridge. Through manipulation of physico-chemical parameters, it was possible to vary nanoparticles in terms of number, shape and size. This is the first report of a transporter protein from a thermophile with the ability to produce nanoparticles in vitro thus expanding the limited knowledge around biological gold nanoparticle synthesis.

Keywords Gold nanoparticles · Thermophilic · Gold reduction · Biological synthesis · ABC transporter

Electronic supplementary material The online version of this article (doi:10.1007/s13404-014-0147-8) contains supplementary material, which is available to authorized users.

M. Erasmus · E. D. Cason · J. van Marwijk · E. Botes · E. van Heerden (✉)
Department of Microbial, Biochemical and Food Biotechnology, Faculty of Natural and Agricultural Sciences, University of the Free State, Bloemfontein 9300, South Africa
e-mail: vheerde@ufs.ac.za

M. Erasmus
e-mail: erasm@ufs.ac.za

E. D. Cason
e-mail: casoned@ufs.ac.za

J. van Marwijk
e-mail: jacquelinevanmarwijk@yahoo.com

E. Botes
e-mail: elsabe75@gmail.com

M. Gericke
Biotechnology Division, Mintek, Private Bag X3015, Randburg 2125, South Africa
e-mail: mariekieg@mintek.co.za

Introduction

Colloidal gold nanoparticles have attracted the interest of scientists for over 400 years, and the synthesis thereof includes reduction of chloroauric acid by reductants; use of these reductants produces particles of relatively uniform size, which are generally spherical [1–3]. In order to control synthesis of these particles, the methodology by which they are produced should be understood. The means by which microorganisms achieve changes in metal speciation and mobility are essential gears of the biogeochemical cycles of metals, as well as for other elements [4]. Microorganisms can interact with metals in a variety of ways [5], [6–8] and biomineralization occurs through one of two major pathways, namely biologically induced biomineralization (BIM) or

boundary-organized biomineralization (BOB) [9]. When the BIM pathway is followed, the organism has little control over deposition of mineral particles and these particles are often characterized by poor crystallinity, broad particle size distribution and non-specific crystal morphology [10–12]. Alternatively, when the BOB pathway is followed, the organism could exercise control over the nucleation and growth of particles. These nanoparticles are developed under the direct regulatory control of the organism and synthesized at a specific location within the cell and only under certain conditions [11–13].

The ability to produce gold nanoparticles with predictable shapes and sizes under controlled conditions could result in interesting new applications that can potentially be utilized in areas such as optics, electronics and biomedicine [14–17]. The benefits of using a biological synthesis system range from the predictable production of uniform metal nanoparticles due to the highly structured activities of microbial cells to environmentally friendly production methods and the ability to produce nanoparticles with unique shapes and composition [18–20]. It is therefore important to gain an understanding of the mechanism of gold accumulation and reduction by bacterial cells on a molecular and cellular level. Identification and analysis of the biopolymers involved in these processes could potentially allow for a process in a cell-free environment, where the size and shape of particles can be regulated to some extent by specific proteins/enzymes [21]. This would also be advantageous from a process point of view, since it would eliminate the need to harvest the nanoparticles formed within the cells, simplifying the process and lowering operation costs.

Different hypotheses have been formulated about the mechanisms involved in gold reduction and nanoparticle synthesis, and these are all based on enzymes with metal reductase (oxidoreduction) abilities [22, 23]. However, the focus on oxidoreductases has overlooked the concept of 'metabolic promiscuity', where a single protein can have a wide range of functions [24, 25] resulting in a lack of knowledge concerning the mechanisms and capabilities of other non-reductase proteins that are still capable of gold reduction and nanoparticle formation [24, 25].

In this paper, the interaction between *Thermus scotoductus* SA-01 and gold chloride ions was evaluated on both a biomass level, where biomass refers to the whole cells of *T. scotoductus* SA-01, and by using a purified protein that was identified to be capable of regulating gold nanoparticle synthesis. The effect of the physico-chemical parameters on particle morphology was assessed, and it was determined whether these parameters can be manipulated to produce size- and shape-specific nanoparticles.

Experimental details

Microorganisms and growth

T. scotoductus SA-01 was always grown from a glycerol stock, plated out onto TYG-agar plates (5 g L^{-1} tryptone, 3 g L^{-1} yeast extract, 1 g L^{-1} glucose and 18 g L^{-1} bacteriological agar) and grown for 24 h. A 20–24-h-old culture was used to prepare the pre-inoculum (a loop full of culture in 50 ml TYG in a 250-ml Erlenmeyer flask) and grown until mid-exponential growth phase (~8 h). The inoculum was also grown to mid-exponential growth phase (~8 h) and was prepared by adding 10 ml of the pre-inoculum to 90 ml TYG (in a 500-ml Erlenmeyer flask). Five millilitres of the inoculum was added to 95 ml TYG (in a 500-ml Erlenmeyer flask) for the growth experiments. One-millilitre samples were withdrawn over time (every 2 h until 16 h, and then at 20 and 24 h), and the optical density (OD) was measured at 600 nm.

The correlation between growth phase and gold reduction was evaluated by collecting biomass at different time intervals as described before. The biomass was washed three times and resuspended in a 1:20 *w*/*v* ratio in 50 mM acetate buffer, pH 5.0 [21]. Au(III), to a final concentration of 2 mM, was added and the concentration determined by using a spectrophotometric method adapted from Melwanki and co-workers [26].

Biomass was obtained as described previously to be used as whole cell catalysts and exposed to varying physico-chemical parameters. The effect of pH was evaluated using a pH ranged from 3.6, 5.5 (50 mM sodium acetate buffer) and 7.4 (50 mM sodium phosphate buffer) to 9.0 (50 mM borax buffer), while gold ion concentration was evaluated for the range starting from 0 to 0.01 M. The temperature range stretched from 30 to 65 °C and the exposure time from 1 to 48 h.

Šlouf and co-workers [27] indicated that gold nanoparticles exhibit pink/purple red colours, which arises due to excitation of surface plasmon vibrations in the gold nanoparticles. UV–Vis spectroscopy can be used to record the surface plasmon band of the gold nanoparticles resulting in visual confirmation (a shift from a yellow to a pink/purple colour) indicative of gold nanoparticle production [28]. Samples were withdrawn over time and a UV–Vis spectrum (400–700 nm) was obtained using a Beckman DU-800 spectrophotometer, to evaluate the plasmon band associated with gold nanoparticles. These samples were also analysed by transmission electron microscopy (TEM), as described below.

Cell-free extraction and protein purification

T. scotoductus SA-01 was grown to the late exponential growth phase [29], biomass harvested by centrifugation (6,000×*g*; 15 min; 4 °C) and cell pellets washed three times with 50 mM sodium phosphate buffer (pH 7.4). Cell-free extracts were prepared according to adapted methods of Gaspard and co-workers

(this implied that the cells were broken to release the proteins from within the cell) [30]. The soluble fraction was size fractionated and concentrated using an Amicon stirred cell fitted with a UF 30 MWCO membrane (Osmonics Inc.). The retentate was dialysed (SnakeSkin 7000 MWCO; Thermo Scientific) against 50 mM sodium phosphate buffer (pH 7.4) to remove reducing agents such as organic acids and carbohydrates. The filtrate was applied to a Super Q-Toyopearl column (TOSOH) in 50 mM sodium phosphate buffer (pH 7.4). The non-binding protein fraction, which was able to form nanoparticles in the presence of $HAuCl_4$, was pooled and dialyzed against 50 mM sodium acetate buffer (pH 5.0). The dialysate was applied to a SP-Toyopearl column (TOSOH) and eluted with a 0–1 M NaCl gradient. Active fractions were pooled, dialysed against 50 mM sodium phosphate buffer (pH 7.4) and reapplied to the SP-Toyopearl column (TOSOH). Bound proteins were eluted with a linear 0–0.3 M NaCl gradient, active fractions pooled and dialysed against 50 mM sodium phosphate buffer (pH 7.4) and applied to a Blue-Sepharose CL-6B column (Sigma-Aldrich). Proteins were eluted with a linear 0–0.6 M NaCl gradient, active fractions pooled and dialysed against 50 mM sodium phosphate buffer (pH 7.4). Ammonium sulphate was added to 1 M and applied to a Phenyl-Toyopearl column (TOSOH) pre-equilibrated with 50 mM sodium phosphate buffer (pH 7.4) containing 1 M $(NH_4)_2SO_4$. Bound proteins were eluted with a linear 1–0 M $(NH_4)_2SO_4$ gradient, active fractions pooled and dialysed against 50 mM sodium phosphate buffer (pH 7.4). The sample was concentrated to ~3 ml and applied to a Sephacryl S200HR column (Sigma-Aldrich) (2.5×65 cm). Proteins were eluted with 50 mM sodium phosphate buffer (pH 7.4) containing 50 mM NaCl at 1 ml min^{-1}. All liquid chromatography procedures were performed on an Äkta Prime Purification System (Amersham Biosciences).

Cloning and expression of protein

N-terminal sequencing of the purified protein was performed by automated Edman degradation with an Applied Biosystems 477A gas-phase sequencer (Foster City, CA) at the Protein Chemistry Facility of the Centro de Investigaciones Biológicas (CSIC; Madrid, Spain). From the obtained sequence, primers were designed and the target gene was PCR amplified with 2 mM $MgCl_2$, 0.8 mM dNTPs, 2.5 U Super-Therm polymerase, 0.2 μM of both the forward (ABC_F_Nde– 5′ CAT ATG AGA AAA GTA GGC AAG CTG GCT 3′) and reverse (ABC_R_Eco – 5′ GAA TTC TTA CTT GAC GGA AAG AGC GTA 3′) primers and 50 ng gDNA template. The gene was cloned into pET-28b(+) and the construct transformed into *Escherichia coli* Rosetta-Gami 2 (DE3) competent cells (Novagen) for expression. The transformants were inoculated into antibiotic-containing LB media (8 g L^{-1} tryptone, 5 g L^{-1} yeast extract, 5 g L^{-1} NaCl and 30 μg L^{-1} kanamycin) and cultured until an OD_{600} of 0.8 was reached before IPTG was added to a final concentration of 1 mM to induce expression. The cells were incubated a further 4 h before being harvested, washed (50 mM sodium phosphate buffer, pH 7.4) and disrupted by ultrasonic treatment. The fractions were separated by ultra-centrifugation (100,000×*g*; 90 min; 4 °C). Purification of the protein was achieved with poly-histidine tag affinity chromatography using a HisTrap FF column (GE Healthcare) according to the manufacturer's instruction and an imidazole gradient ranging from 20 to 500 mM (100 ml; flow rate, 5 ml min^{-1}). Fractions were examined by Coomassie staining following SDS-PAGE [31, 32], and those containing proteins of approximately 70 kDa were pooled and further fractionated by size exclusion chromatography at a flow rate of 1 ml min^{-1} on Sephacryl S200HR (Sigma-Aldrich). Active fractions were pooled and dialyzed against 50 mM sodium phosphate buffer (pH 7.4), with Snakeskin-Pleated dialysis tubing (10000 MWCO, Thermo Scientific) at 4 °C with two 2 L buffer change. Protein concentrations were determined using the BCA™ Protein Assay Kit (PIERCE–Thermo Scientific).

Gold reduction and nanoparticle synthesis using cell-free extracts and purified protein

Proteins present in cell-free extracts were routinely assayed for gold reducing ability by incubating the sample with 2 mM $HAuCl_4$ in 50 mM sodium phosphate buffer (pH 7.4) at 65 °C for 24 h. Nanoparticle synthesis using the purified protein was performed under the same reaction conditions but with 4.6 μM sodium dithionite [33] added as a reducing agent [34]. In a living cell, natural reductants are present that are capable of reducing co-factors and in this case the disulphide bridge present in the protein, but these are absent in the purified protein fractions; thus, the reductant facilitates the reduced state of the protein. The sodium dithionite reduces the disulphide bridge in the protein, therefore enabling the protein to reduce the gold ions.

To assess the influence on the size and shape of nanoparticles, reaction mixtures were prepared as follows: $HAuCl_4$ was added to 0.5, 2, 10 and 20 mM; protein concentrations were varied from 10–100 μg ml^{-1} and sodium dithionite from 0–100 μM. Incubation times ranged from 2 to 48 h, temperatures from 30–75 °C and pH ranged from 3.6, 5.5 (sodium acetate buffer) and 7.4 (sodium phosphate buffer) to 9.0 (borax buffer). Formation of a pink/purple colour indicated gold nanoparticle production [27], which was confirmed with TEM analysis, as described below.

Transmission electron microscopy

Biomass samples were prepared for TEM analysis by separating the whole cells from the liquid by centrifugation. The biomass was washed twice in 0.1 M phosphate buffer, pH 7.0 and fixed overnight in 3 % glutaraldehyde solution, prepared

in sodium phosphate buffer, pH 7.0. Recovering and washing of the biomass were done by centrifugation. The biomass was enrobed in 1 % agar and dehydrated in a graded acetone-water series. Infiltration and embedding were accomplished by spurr-epoxy resin, followed by two changes of spurr. Blocks were polymerized at 70 °C for 8 h and the embedded material sectioned with an ultra-microtome, yielding sections of approximately 0.2 μm which were mounted on copper grids.

For the cell-free extracts and the purified protein, a drop of the sample was placed onto carbon-coated formvar grids; excess sample was removed after a minute using blotting paper, and the grids were air-dried before analysis. The appropriate controls were evaluated without protein or sodium dithionite to compensate for chemical reduction.

Electron micrographs were taken with either a Philips CM 100 or 200-kV Philips CM 20 TEM [35]. Elemental analysis was carried out using energy-dispersive X-ray spectroscopy (EDS) attached to the TEM.

X-ray diffraction

X-ray diffraction (XRD) analysis was conducted by the Geology Department at the University of the Free State. The data was collected at 40 kV and 30 mA with a Siemens D 8000 diffractometer using CuKά radiation.

Results and discussion

Nanoparticle formation using *T. scotoductus* SA-01 whole cells

T. scotoductus SA-01 is unique to South Africa and can reduce a number of compounds as electron acceptors through dissimilatory pathways. These compounds include Fe(III), Mn(IV), Co(III)-EDTA, Cr(VI) and U(VI) [36]. The Au(III) reducing capability of *T. scotoductus* SA-01 cells in different growth phases illustrated that maximum Au(III) removal or reduction was reached after 8 h, which corresponds to the late exponential—early stationary growth phase (Fig. 1a). When these cells were incubated in the presence of Au(III), ultra-thin section transmission electron microscopy (TEM) revealed that the gold was mainly deposited on the outer wall layer (Fig. 1b) and elemental analysis, using EDS, showed that the particles do consist of gold (Fig. 2a); also present in vast amounts are copper and carbon which can be attributed to the copper grid and the cell biomass. Since nanoparticle synthesis was associated with the biomass, it may be concluded that the cells might have a higher degree of control over the particle morphology as the BOB pathway of mineralization is observed [10–12]. XRD analysis on the biomass exposed to gold ions gave an XRD pattern of the gold precipitated in or on the bacterial cells showing distinct peaks corresponding to the (111); (200) and (220) Bragg reflections of gold [37] (Fig. 2b) which confirms the EDS results.

Effect of the physico-chemical parameters on nanoparticle formation

Various physico-chemical parameters were evaluated using whole cell biomass to determine their effect on gold reduction and nanoparticle formation. These parameters included pH, temperature, exposure time and gold ion concentration. The particle formation was confirmed visually through colour formation (Supplementary figure 1c), peaks observed on the UV–Vis (400–700 nm) spectra (Supplementary figures 1a and b) and TEM analysis. An increase in the size of nanoparticles results in a change of colour, from pink, to purple, to

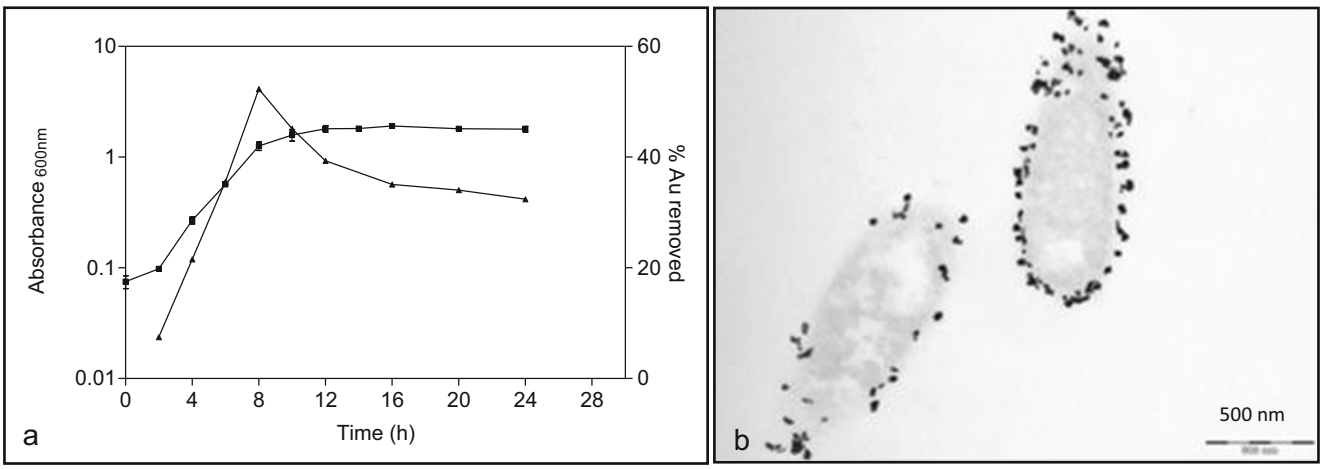

Fig. 1 Interactions of *Thermus scotoductus* SA-01 with Au(III). **a** Growth curve for *T. scotoductus* SA-01, showing the correlation between growth phase (*square*) and Au(III) removal (*triangle*). **b** Thin section TEM micrograph of *T. scotoductus* SA-01 exposed to 2 mM $HAuCl_4$; the micrograph shows the presence of gold deposited along the outer wall layer

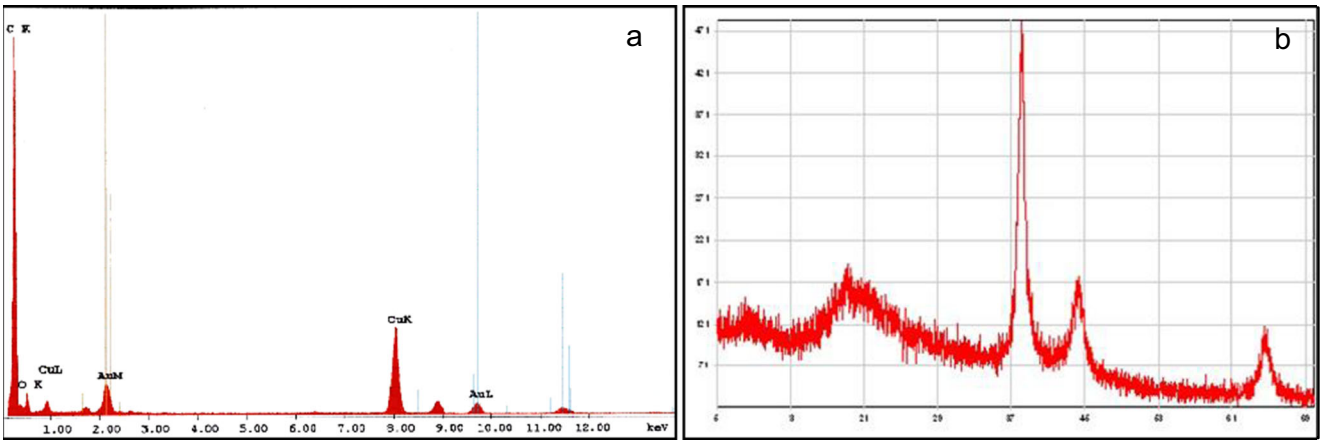

Fig. 2 **a** EDS analysis and **b** XRD pattern recorded of *T. scotoductus* SA-01 cells incubated in the presence of 2 mM Au(III)

blue, due to the surface plasmon vibrations of the gold nanoparticles [38].

The effect of pH on the production of nanoparticles indicated that a lower pH was more conducive to the formation of larger particles while a higher pH resulted in the formation of small particles (Fig. 3a, b). Although pH does affect the size, shape and location of the particles, contrary to suggestions by He and co-workers, particle shape and distribution could not be controlled at this level [21]. In Fig. 3a, the formation of octahedral gold is observed and this points to mineral diagenesis, while intracellular gold reduction leads to cell death (Supplementary figure 2) versus Fig. 3b where immobilization is focused in the cell envelope. Temperature and exposure time had no significant effect on particle morphology but influenced the amount and rate of particle formation. Lower temperatures and shorter incubation periods resulted in fewer particles formed where an increase in temperature and longer incubation periods resulted in more and slightly larger particles. These findings agree with the physico-chemical properties of nanoparticles as discussed by Gericke and Pinches [39] who stated that the rate of particle formation can be correlated with the incubation temperature where an increase in temperature will allow faster particle formation and the rate of reduction can influence the type of particle formed.

Figure 4 illustrates the effect of gold ion concentration on particle formation. At concentrations exceeding 5 mM (for example 10 mM seen in Fig. 4b), the cells are ruptured by the nanostructures formed and are released into the environment and all means of controlling particle morphology is lost. Gold ion concentrations lower than 5 mM (for example 0.5 mM as seen in Fig. 4a) result in the formation of smaller particles which are associated with the biomass. The effect of gold ion concentration on particle formation at various concentrations can be seen in supplementary Fig. 3a to e.

Nanoparticles from cell-free extracts

Incubation of soluble proteins >30 kDa with $HAuCl_4$ resulted in the formation of nanoparticles and also showed a correlation between Au concentration and types of nanoparticles synthesized (Fig. 5). Similar observations were also made by Li and co-workers [15], Shankar and co-workers [17] and Wei and co-workers [40] where it was demonstrated that gold nanosheets with triangular, hexagonal or truncated shapes were dependent on the reductant to Au ion ratio. A mixture of small amorphous particles and nebula-like formations were observed at low Au(III) concentrations (Fig. 5a), but with some particles with specific shapes at 5 mM (Supplementary

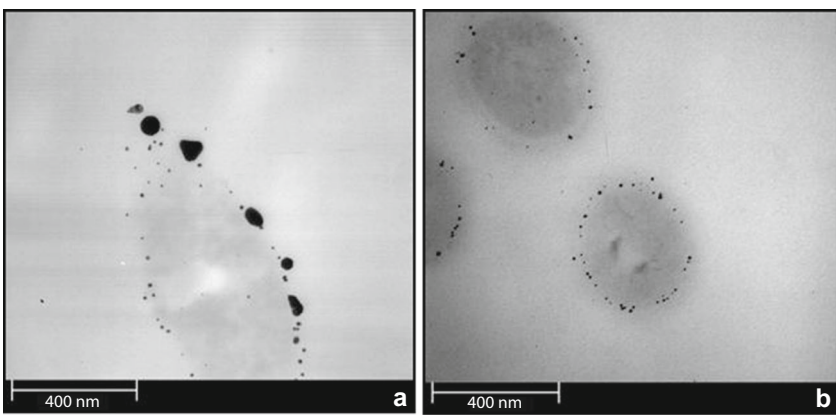

Fig. 3 TEM micrographs illustrating the effect of pH **a** 3.6 and **b** 9.5 on particle formation using whole cell biomass

Figure 4a). Addition of 10 and 20 mM Au(III) resulted in large particles (Supplementary Figure 4b and Figure 5b), with definite crystalline surfaces. Morphologies were nanosheet-like, with shapes being mostly triangular and hexagonal. Nanosheets were crystalline with no twinning present and a prominent herring motif. The triangular nanosheets showing threefold symmetry were in the {111} orientation (data not shown), and dark lines visible through the crystals (Fig. 5b) are likely bend contours [41].

Nanoparticles from purified protein

A protein from *T. scotoductus* SA-01, able to catalyse and direct the synthesis of gold nanoparticles, was purified to homogeneity. It was determined to have a molecular mass of ~70 kDa (Supplementary Figure 5), and Edman degradation resolved the N-terminal sequence as GPQDNSLVIGAS which showed 100 % homology with the ABC transporter peptide-binding protein (YP_004203474) from *T. scotoductus* SA-01 [42] and *T. thermophilus* (AEG34049). These types of proteins are ubiquitous membrane proteins that facilitate unidirectional substrate translocation across the lipid bilayer by utilizing the energy obtained from the hydrolysis of ATP and have been found to be very diverse with respect to their physiological function and substrate unlike oxidoreductases which mainly catalyse oxidation-reduction reactions coupled to NADP/NAD^+ utilization [43–45].

Subsequent cloning and sequencing of the gene revealed the presence of a disulphide bond (between amino acid 337C and 481C) which confirms the hypothesis of Scott and co-workers [34], implicating an electron shuttle mechanism via a reduced disulphide bridge. This is further supported by the work done by Cason and co-workers [46] who found that reduction of the disulphide bonds resulted in electron transfer to a metal, in their case U(VI). Furthermore, a decrease in U(VI) reduction was observed when the disulphide bridge of the same ABC transporter peptide-binding protein was disrupted by mutation of the genes involved.

According to Tang and Hamley [47], nanostructures can be formed when Au(III) is gradually reduced to Au(I), and when this reduction is almost complete, the equilibrium shift towards reduction of Au(I) to Au(0). This, in turn, leads to the formation of nucleation sites that initiates nanoparticle synthesis. Nucleation sites gradually grow into more complex structures when sufficient Au(I) ions are present. The crystallization of gold is directed by the reducing as well as the stabilizing agent. It is shown that the reduced protein, purified from *T. scotoductus* SA-01, reduces Au(III) to elemental gold and acts as a stabilizing agent that directs the shape and size of the synthesized nanoparticle. To demonstrate this ability, the purified protein was used to evaluate the effects of various physico-chemical parameters on $HAuCl_4$ reduction and subsequent nanoparticle formation, further validated by no nanoparticle formation with protein-free controls.

Particle synthesis manipulations

Au(III): reductant ratio

Significant reduction of Au(III) only occurred in the presence of the proteins from cell-free extracts and once purified only when sodium dithionite was added to the reaction to keep the protein in its reduced form, thus confirming the disulphide electron shuttle mechanism. This was shown by Cason and co-workers [46] as well as Scott and co-workers [34]. Varying dithionite concentrations revealed that a stoichiometric ratio of less than 1:1 (4.6 μM sodium dithionite to protein) resulted in particles with defined edges.

Similar to the cell-free extracts, the purified protein produced small, amorphously shaped particles at low Au(III) concentrations (Fig. 6a), but exposure to higher Au(III) concentrations led to the formation of plate-like nanostructures (Fig. 6b). Varying protein concentrations confirmed the importance of Au(III) to protein (reductant) ratio, where high protein concentrations resulted in small, undefined nanoparticles and low protein concentrations in bigger particles with defined edges.

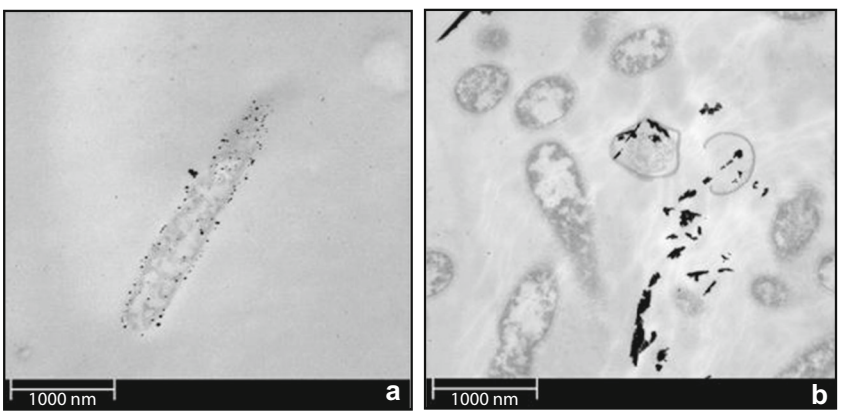

Fig. 4 TEM micrographs illustrating the effect of Au(III) concentration **a** 0.5 and (**b**) 10 mM on particle formation using whole cell biomass

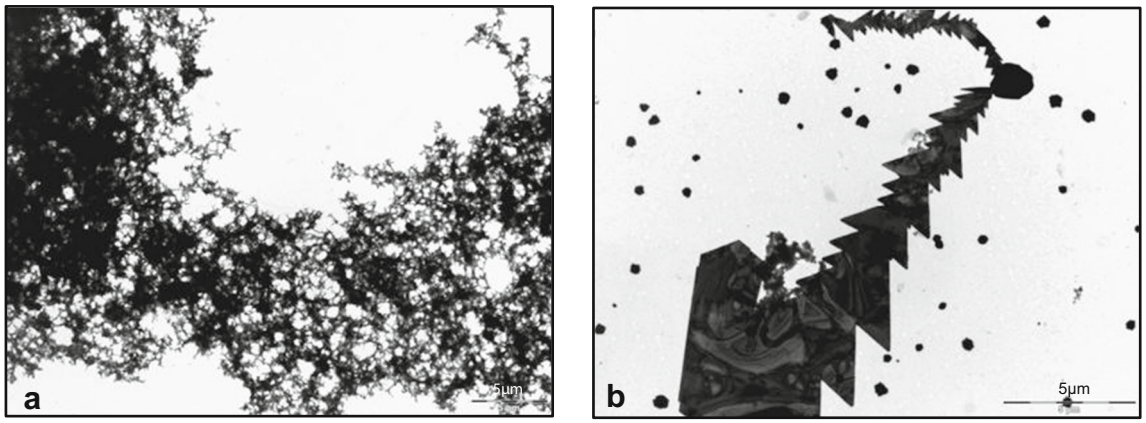

Fig. 5 Nanoparticle formation with >30 kDa soluble fraction proteins with varying $HAuCl_4$ concentrations. **a** 2 mM and **b** 20 mM

At high reductant to Au(III) ratios, gold ions are preferentially committed to particle initiation (nucleation) rather than particle growth [47] resulting in higher numbers of small particles. However, at lower reductant to Au(III) ratios, fewer nucleation sites are available for particle initiation which allows for bigger particles to grow as there is less competition for available gold ions [33, 48]. Thus, the less nucleation sites are available, and the bigger particles can grow as there will be less competition for gold ions to act either as part of the nucleation process or to grow the size of the particle.

Incubation time, temperature and pH

Nanoparticles were already formed after only 8 h of incubation, but longer reaction times (up to 48 h) only resulted in higher numbers of particles and did not have a significant effect on particle size. Since Au(III) reduction and eventual nanoparticle synthesis are time-dependent reactions, longer incubation times allow for the reaction equilibrium to shift towards Au(I) reduction and formation of more nucleation sites. With longer incubation times, more nucleation sites can be occupied leading to higher numbers of particles [47, 48].

Temperature had no effect on the size of the nanoparticles, but did influence particle shape. Incubation at lower temperature resulted in fewer particles but with defined edges (Fig. 7a), while particles produced at 75 °C were mostly spherical (Fig. 7b). The overall effect of temperature is likely in influencing the nucleation seed, rather than particle growth [49].

Lower pH values were more conducive to producing nanoplate-like structures with a larger aspect ratio (Fig. 8a and Supplementary Figure 6a), while incubation at higher pH resulted in more small spherical particles (Supplementary Figure 6b). Particles with defined edges were formed at pH 7.4 (Fig. 8b). Different pH values regulate the effective proton concentration of the solution, which in turn controls

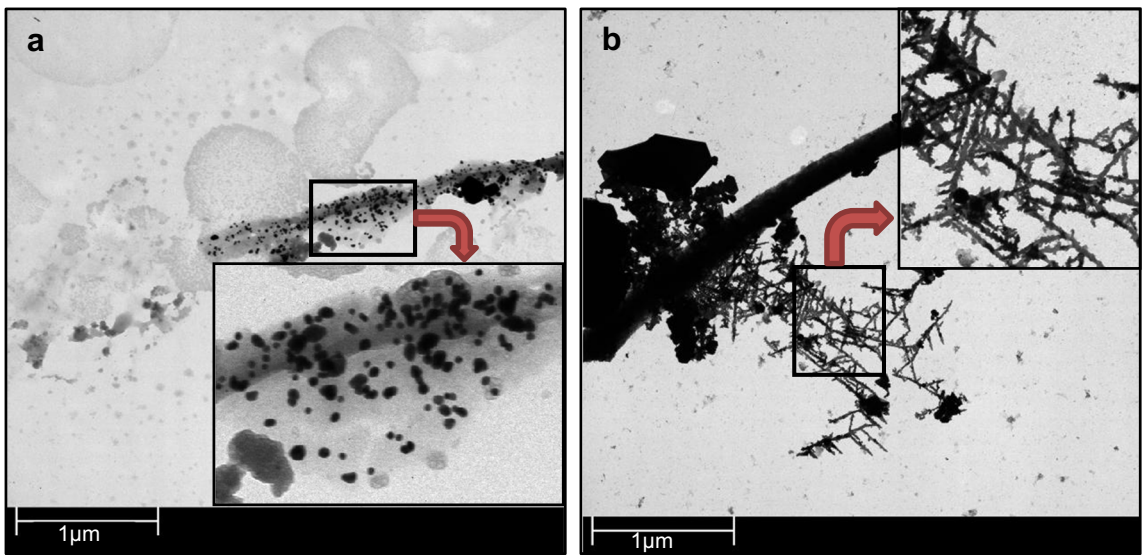

Fig. 6 TEM micrographs showing the effect of $HAuCl_4$ concentration **a** 0.5 mM and **b** 10 mM, on nanoparticle formation in the presence of purified protein

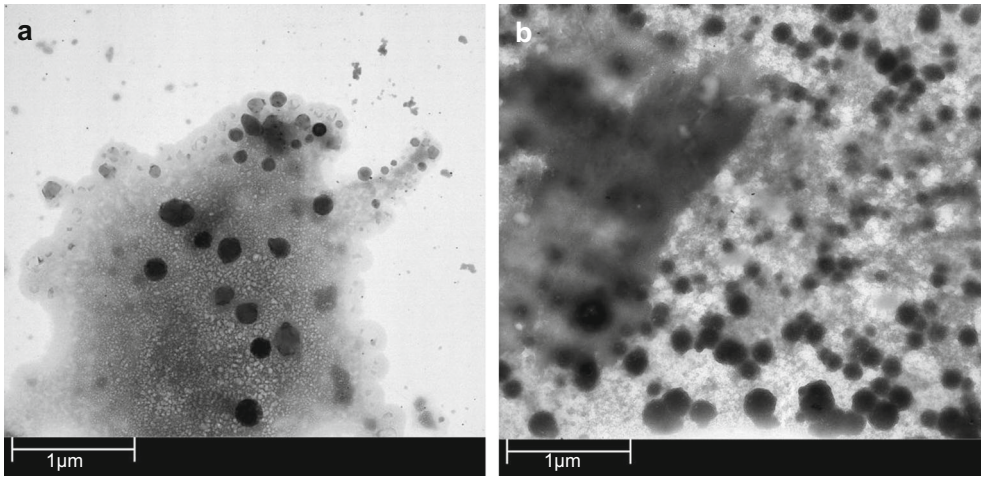

Fig. 7 TEM micrographs of nanoparticles formed at **a** 42 °C and **b** 75 °C with purified protein

nanoparticle morphology rather than affecting nucleation and particle initiation N.

Conclusions

T. scotoductus SA-01, the thermophilic bacterium used in this study, has the ability to reduce Au(III) and produce nanoparticles, making it a suitable candidate for the production of nanoparticles.

In this study, it was found that the physico-chemical parameters have a definite influence on particle size with lower pH and higher temperatures resulting in larger particles and in contrast, higher pH and lower temperatures will produce smaller particles. However, these processes are difficult to control and a predefined morphology is still unobtainable at this time. Microorganisms are very complex structures with a variety of metabolic functions which all contribute towards the proper working of the cell. Many of these activities could be involved in the reduction of gold and the formation of nanoparticles, but a better understanding of the mechanism might be obtained if the protein/s involved in these reactions is elucidated. Gold reduction primarily occurred in the cell envelope which is strong evidence for a gold 'specific' reduction process, hinting at a location for further investigation.

An ABC transporter, peptide-binding protein of *T. scotoductus* SA-01, able to reduce and synthesize gold nanoparticles was purified to homogeneity. Even though this type of protein is not a classical oxidoreductase, a cysteine–disulphide bridge electron shuttle mechanism is likely involved in reducing Au(III). Moreover, the protein also acts as nucleation seed sites that initiate and direct nanoparticle synthesis. Through manipulation of physico-chemical parameters, it is clear that particle formation can be influenced in terms of size, shape and number of particles formed. However, since biological Au(III) reduction and nanoparticle synthesis is a complex process, manipulations of single parameters are

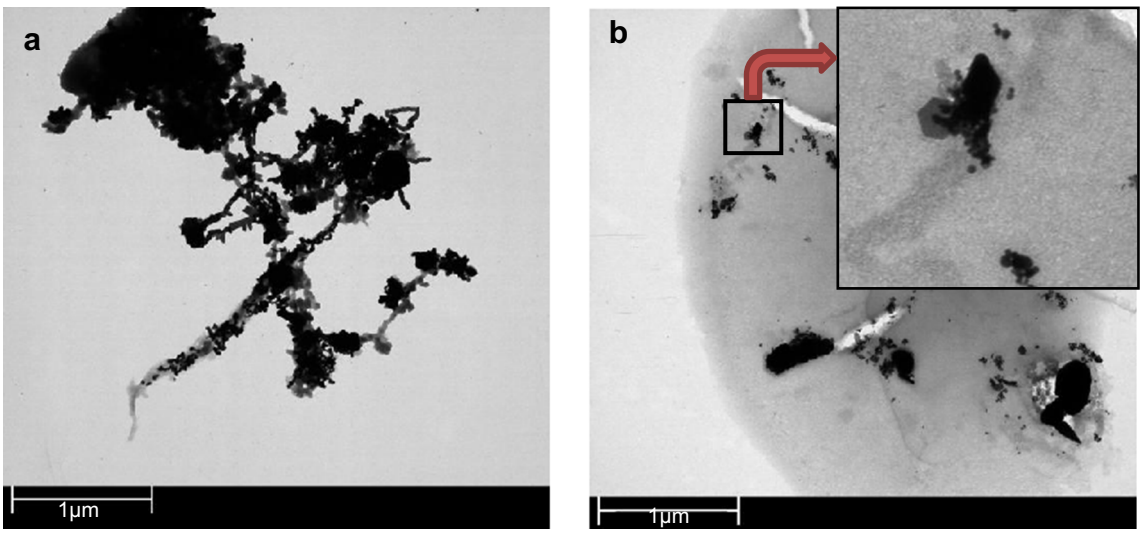

Fig. 8 TEM micrographs of nanoparticles formed at varying pH. **a** pH 5.5 and **b** pH 7.4 with purified protein

unlikely to result in the best conclusive results. This is witnessed by a lack of particle monodispersity (with the exception of small spherical particles) when evaluating any of the parameters. Varying and investigating multiple parameters simultaneously will likely shed light on the way forward to controlling and directing biological nanoparticle synthesis.

Acknowledgments This work was funded by the Project AuTek initiative and Mintek, which we gratefully acknowledge and thank for permission to publish this paper. We also thank Gordon Southam (University of Western Ontario, Canada) for his help with the TEM analysis and interpretation of the micrographs and Liesl van der Westhuizen (University of the Free State) for her assistance in the preparation of this manuscript. We also acknowledge the microscope centres at the following universities and the personnel for their help with the TEM and EDS analysis: University of the Free State, South Africa; University of Western Ontario, Canada; Nelson Mandela Metropolitan University, South Africa and the University of Ghent, Belgium.

Author contributions All work done in this manuscript is based on results from a PhD thesis by JvM with supervision by EvH. The manuscript was written by ME and EDC with input from JvM, EB and EvH. Monetary support for this work was supplied by MG from Mintek as well as NRF funding from EvH research grants.

References

1. Masala O, Seshadri R (2004) Annu Rev Mater 34:41–81
2. Handley DA (1989) Colloidal gold: principles, methods and applications. Volume 1, 13th edn. Academic, San Diego, 33
3. Sau TK, Pal A, Pal T (2001) J Phys Chem 105:9266–9272
4. Gadd GM (2001) Curr Opin Biotechnol 11:271–279
5. Ahmann D, Roberts AL, Krumholz LR, Morel FM (1994) Nature 371:750
6. Klaus-Joerger T, Joerger R, Olsson E, Granqvist CG (2001) Trends Biotechnol 19:15–20
7. Nies DH (1999) Appl Environ Biotechnol 51:730–750
8. Spain A (2003) Rev Undergrad Res 2:1–6
9. Mann S (1993) Nature 365:499–505
10. Weiner S, Dove PM (2003) Rev Mineral Geochem 54:1–29
11. Frankel RB, Bazylinski DA (2003) Rev Mineral Geochem 54:95–114
12. Frankel RB, Bazylinski DA (2003) Rev Mineral Geochem 54:217–247
13. Veis A (2003) Rev Mineral Geochem 54:249–289
14. C.W. Corti, R.J. Holliday and D.T. Thompson, First nanofabrication symposium, Ireland, (2004)
15. Li C, Cai W, Cao B, Sun F, Li Y, Kan C, Zhang L (2006) Adv Funct Mater 16:83–90
16. Kim J, Cha S, Shin K, Jho JY, Lee J (2004) Adv Mater 16:459–464
17. Shankar SS, Rai A, Ahmad A, Sastry M (2005) Chem Mat 17:566–572
18. Ahmad A, Mukherjee P, Mandal D, Senapati S, Khan MI, Kumar R, Sastry M (2002) J Am Chem Soc 124:12108–12109
19. Mukherjee P, Senapati S, Mandal D, Ahmad A, Khan MI, Kumar R, Sastry M (2002) ChemBioChem 5:461–463
20. Sastry M, Ahmad A, Khan MI, Kumar R (2003) Curr Sci 85:162–170
21. He S, Zhang Y, Guo Z, Gu N (2008) Biotechnol Prog 24:476–480
22. Duran N, Marcato PD, Alves OL, De Souza GIH, Esposito E (2005) J Nanobiotechnol 3:8–14
23. He S, Guo Z, Zhang Y, Zhang S, Wang J, Gu N (2007) Mater Lett 61:3984–3987
24. Van Heerden E, Opperman DJ, Bester PA, van Marwijk J, Cason ED, Litthauer D, Piater LA, Onstott TC (2008) Proc SPIE - Int Soc Opt Eng 7097:70970S
25. Khersonsky O, Tawfik DS (2010) Annu Rev Biochem 79:471–505
26. Melwanki MB, Masti SP, Seetharamappa J (2002) Turk J Chem 26:17–22
27. Šlouf M, Kužel R, Matej Z (2006) Krist Suppl 23:319–324
28. Lazarides AA, Schatz GC (2000) J Phys Chem B 104:460–467
29. Opperman DJ, van Heerden E (2007) J Appl Microbiol 103:1907–1913
30. Gaspard S, Vazquez F, Holliger C (1998) Appl Environ Microbiol 64:3188–3194
31. Fairbanks G, Steck TL, Wallach DFH (1971) Biochemistry 10:2606–2617
32. Lamelli UK (1970) Nature 227:680–685
33. Showe MK, DeMoss JA (1968) J Bacteriol 95:1305–1313
34. Scott D, Toney M, Muzikar M (2008) J Am Chem Soc 130:865–874
35. van Wyk PWJ, Wingfield MJ (1991) Mycologia 83:698–707
36. Kieft TL, Fredrickson JK, Onstott TC, Gorby YA, Kostandarithes HM, Bailey TJ, Kennedy DW, Li SW, Plymale A, Spadoni CM, Gray MS (1999) Appl Environ Microbiol 65:1214–1221
37. Leff DV, Brandt L, Heath JR (1996) Langmuir 12:4723–4730
38. Corti CW, Holliday RJ, Thompson DT (2002) Gold Bull 35:111–117
39. Gericke M, Pinches A (2006) Hydrometallurgy 83:132–140
40. Wei D, Qian W, Shi Y, Ding S, Xia Y (2007) Carbohydr Res 342:2494–2499
41. Rodriguez-Gonzalez B, Pastoriza-Santos I, Liz-Marzan LM (2006) J Phys Chem B 110:11796–11799
42. Gounder K, Brzuszkiewicz E, Liesegang H, Wollherr A, Daniel R, Gottschalk G, Reva O, Kumwenda B, Srivastava M, Bricio C, Berenguer J, van Heerden E, Litthauer D (2011) BMC Genomics 12:577–590
43. Braibant M, Gilot P, Content J (2000) FEMS Microbiol Rev 24:449–467
44. Locher KP, Broths E (2004) FEBS Lett 564:264–268
45. Saurin W, Hofnung M, Dassa E (1999) J Mol Evol 48:22–41
46. Cason ED, Piater LA, van Heerden E (2012) Chemosphere 86:572–577
47. Tang T, Hamley IW (2009) Colloid Surf A 336:1–7
48. Mikheenko IP, Rousset M, Dementin S, Macaskie LE (2008) Appl Environ Microbiol 74:6144–6146
49. Kawamura G, Nogami M (2009) J Cryst Growth 311:4462–4466